

# Reactive Power Distribution Strategy and Droop Control Method Based on Virtual Impedance in Microgrid

Xue-Long Li, Shuang Zhao, Jie-Sheng Wang \*, An He

**Abstract**—The control mode of microgrid is generally divided into micro source level control, system level control and dispatching level control. This paper mainly studies the equivalent structure of the AC microgrid system, and proposes the reactive power distribution strategy and droop control method of the AC microgrid based on virtual impedance under off-grid operation mode by analyzing the voltage relationship between the reactive power output of the microgrid and the AC bus. The droop control is used to realize the equal distribution of reactive power. It is necessary to ensure that the product of capacity and line impedance parameters of micro source converter is constant. Due to inconsistent line impedance, when the traditional droop control strategy is applied in the voltage regulation, the reactive power can't be distributed according to its capacity. So the microgrid droop control strategy based on virtual impedance is proposed by introducing virtual impedance controller. The control layer and the electrical layer make the line impedance meet the conditions of the proportional distribution of reactive power so as to achieve the optimal regulation of the microgrid voltage. The simulation results show that the reactive power distribution strategy and droop control method based on virtual impedance can realize the equal distribution of reactive power of each micro source converter in off-grid operation mode, which can ensure that the microgrid has a large voltage adjustment margin.

**Index Terms**—AC microgrid; Reactive power distribution; Virtual impedance; Droop control

## I. INTRODUCTION

ENERGY is an important material basis for social development, and reliable electricity supply is crucial to support the construction of modern civilization. Electricity is the most important secondary energy and sent to the user side

Manuscript received December 4, 2019; revised February 5, 2020. This work was supported by the Basic Scientific Research Project of Institution of Higher Learning of Liaoning Province (Grant No. 2017FWDF10), and the Project by Liaoning Provincial Natural Science Foundation of China (Grant No. 20180550700).

Xue-Long Li is a postgraduate student in the School of Electronic and Information Engineering, University of Science and Technology Liaoning, Anshan, 114051, PR China (e-mail: lx117346536920@126.com).

Shuang Zhao is an engineer of Anshan Power Supply Company, State Grid Liaoning Electric Power Co. LTD., Anshan, 114051, PR China (e-mail: 857111565@qq.com).

Jie-Sheng Wang is with the School of Electronic and Information Engineering, University of Science and Technology Liaoning, Anshan, 114051, PR China; National Financial Security and System Equipment Engineering Research Center, University of Science and Technology Liaoning. (Corresponding author, phone: 86-0412-2538355; fax: 86-0412-2538244; e-mail: wang\_jiesheng@126.com).

An He is an engineer of Anshan Power Supply Company, State Grid Liaoning Electric Power Co. LTD., Anshan, 114051, PR China (e-mail: 54hean@163.com).

by various substations, transmission and distribution networks [1]. Currently, the global energy Internet promoted by state grid corporation is becoming an important comprehensive intelligent electrical platform for China to promote energy industry upgrading, high-end power equipment construction and advanced power grid control optimization technology. Energy Internet not only contains traditional power system, but also has advanced electronic power system [2]. Considering the operation characteristics of distributed power generation equipment, especially its uncertainty and randomness, electromagnetic coupling of power system, power flow calculation, load prediction and relay protection will be the hot spots of future research [3]. The structure of the microgrid depends on how the distributed generation devices and loads are connected to the AC and DC bus of the microgrid system. Microgrid can be divided into AC hybrid, DC hybrid, and AC-DC hybrid microgrid. In the AC hybrid microgrid, various distributed generation units and renewable energy units are connected to the AC bus through their power interface converters [4-6].

For the operation of AC-DC hybrid microgrid, microgrid control strategy and power management scheme are the most important research directions [7]. AC hybrid microgrid control strategies can be divided into grid-connected control strategies and off-grid control strategies [8]. In grid-connected mode, the power management strategy can be divided into dispatching power mode and unassigned output power mode. In the distributed output power mode, the distributed generation units and renewable energy units operate in the power control mode [9-10]. Power control can be achieved by current control or voltage control. Current control mode is the common used grid-connected operation control mode at present, which controls the output current of distributed generation units and renewable energy units so as to track and determine the grid of reference power, output voltage and frequency [11]. In the voltage control mode, both the distributed generation units and the renewable energy units can operate and control the output voltage, whose regulating the output power of the distributed equipment is similar to the synchronous generator in the power system [12]. In off-grid mode, the power management strategies of microgrid mainly include voltage regulation, frequency regulation, reactive power regulation and active power regulation [13-14]. The secondary regulation of frequency and voltage can bring the voltage and frequency of the microgrid back to the stable operation range from the verge of collapse, which can enhance the stability of the microgrid [15]. The reactive power and active power regulation are the

basis to ensure the stability of voltage and frequency of microgrid [16]. In addition, the off-grid switching strategy is also an important research point, which can ensure the synchronization of voltage, frequency and phase between the microgrid and the main grid [17]. General reactive power sharing strategies can be divided into communication-based reactive power regulation and non-communication-based reactive power regulation [18-19].

The control modes of microgrid are generally divided into micro-source-level control, system-level control and dispatching level control [20-21]. This paper mainly studies the reactive power distribution strategy and droop control method of microgrid based on virtual impedance under off-grid operation mode of AC microgrid in off-grid mode, whose main purpose is to ensure the stable margin of microgrid voltage regulation. The structure of the paper is described as follows. Section 2 introduces the simplified structure of multi-energy system of microgrid. Section 3 introduces the reactive power and voltage management of microgrid. Section 4 is the droop control strategy based on virtual impedance. Section 5 is the experimental simulation and result analysis. Final section is the conclusion of the paper.

## II. SIMPLIFIED STRUCTURE OF MULTIPLE ENERGY SYSTEM OF MICROGRID

The key to the stable operation of the microgrid system is to ensure that the voltage and frequency at the AC Bus are within a stable range, the general frequency fluctuation range is  $\pm 0.5\text{Hz}$ , and the voltage fluctuation range is  $\pm 10\%$ . To ensure the stable operation of the microgrid is to ensure the system power balance, that is to say that the power provided by the micro source and the load demand power remain stable so that the voltage and frequency at the AC bus will remain stable. The operation mode of AC microgrid is divided into grid-connected operation and off-grid operation. Under grid-connected, the AC bus is connected to the distribution

network through circuit breakers, and the voltage and frequency at the AC bus are controlled by the distribution network.

Under the off-grid operation, the circuit breaker of the AC bus is disconnected, and the voltage and frequency at the AC bus are adjusted by each micro source in the microgrid. When the microgrid is switched from grid-connected operation mode to off-grid operation mode, the circuit breaker at the AC bus is disconnected, and the AC microgrid is operated in off-grid mode. When the microgrid is switched from off-grid operation mode to grid-connected operation mode, the voltage and frequency at the AC bus should be adjusted to keep it consistent with the distribution network. The circuit breaker can be closed to make it work in the grid-connected operation mode.

The simplified structure of AC microgrid is shown in Fig. 1. When  $n$  micro-sources are connected to the AC bus by independent micro-source converters, the output power of micro-source 1 is  $[v_{a1} \ v_{b1} \ v_{c1}]$  and  $[i_{a1} \ i_{b1} \ i_{c1}]$ , The line impedance is  $Z_1$ , and so on, the output power of micro source  $n$  is  $[v_{an} \ v_{bn} \ v_{cn}]$  and  $[i_{an} \ i_{bn} \ i_{cn}]$ , and the line impedance is  $Z_n$ .

Suppose the output voltage of distributed generation unit is  $[v_a \ v_b \ v_c]$  and  $[i_a \ i_b \ i_c]$ , then the output power of the distributed generation unit is calculated by:

$$S = P + jQ = v_a i_a + v_b i_b + v_c i_c \tag{1}$$

Eq. (1) is the power calculation method of distributed power generation unit in the static coordinate system, but this calculation method is relatively complex. The output voltage and current are sinusoidal functions, and there is an Angle difference. Therefore, the active and reactive power of distributed generation units are generally calculated in the rotation coordinate system. The power calculation of three-phase micro-source converter in the rotating coordinate system requires the following steps:

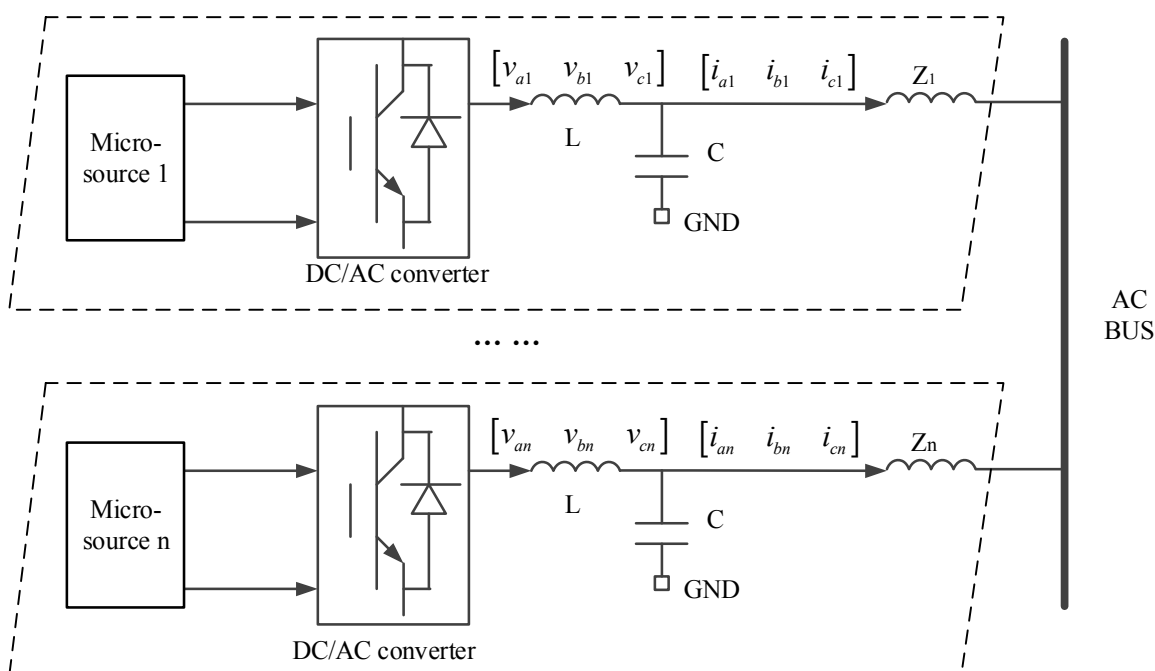


Fig. 1 The simplified architecture of AC microgrid.

1) Voltage and current parameters are converted to the two-phase static coordinate system.

$$\begin{bmatrix} v_\alpha \\ v_\beta \\ v_0 \end{bmatrix} = \begin{bmatrix} 1 & -\frac{1}{2} & -\frac{1}{2} \\ 0 & \frac{\sqrt{3}}{2} & -\frac{\sqrt{3}}{2} \\ 1 & 1 & 1 \end{bmatrix} \begin{bmatrix} v_a \\ v_b \\ v_c \end{bmatrix} \quad (2)$$

$$\begin{bmatrix} i_\alpha \\ i_\beta \\ i_0 \end{bmatrix} = \begin{bmatrix} 1 & -\frac{1}{2} & -\frac{1}{2} \\ 0 & \frac{\sqrt{3}}{2} & -\frac{\sqrt{3}}{2} \\ 1 & 1 & 1 \end{bmatrix} \begin{bmatrix} i_a \\ i_b \\ i_c \end{bmatrix} \quad (3)$$

2) Voltage and current parameters are converted to the two-phase rotating coordinate system.

$$\begin{bmatrix} v_d \\ v_q \end{bmatrix} = \begin{bmatrix} \cos \theta & \sin \theta \\ -\sin \theta & \cos \theta \end{bmatrix} \begin{bmatrix} v_\alpha \\ v_\beta \end{bmatrix} \quad (4)$$

$$\begin{bmatrix} i_d \\ i_q \end{bmatrix} = \begin{bmatrix} \cos \theta & \sin \theta \\ -\sin \theta & \cos \theta \end{bmatrix} \begin{bmatrix} i_\alpha \\ i_\beta \end{bmatrix} \quad (5)$$

After the above transformation, the apparent output power of the distributed generation unit can be expressed as:

$$S = P + jQ = \frac{3}{2}(v_d i_d + v_q i_q) + j \frac{3}{2}(v_q i_d - v_d i_q) \quad (6)$$

### III. REACTIVE POWER AND VOLTAGE MANAGEMENT OF MICROGRID

Fig. 2 shows the control structure diagram of each micro source in AC microgrid under off-grid operation mode, in which each micro source is represented by micro source 1, micro source 2 and micro source  $n$ , and the line impedance of each micro source to the AC bus is represented by  $X_1$ ,  $X_2$  and  $X_n$ , while each micro source adopts the droop control strategy. The active power  $P_i$  and reactive power  $Q_i$  of each micro source in the microgrid can be expressed as:

$$\begin{cases} P_i = \frac{1}{Z_i}(EV_i \cos \theta_i \cos \varphi_i - E^2 \cos \varphi_i + EV \sin \theta_i \sin \varphi_i) \\ Q_i = \frac{1}{Z_i}(EV_i \cos \theta_i \sin \varphi_i - E^2 \sin \varphi_i + EV_i \sin \theta_i \cos \varphi_i) \end{cases} \quad (7)$$

Simplify Eq. (7) to obtain:

$$\begin{cases} P_i = \frac{EV_i}{X_i} \theta_i \\ Q_i = \frac{EV_i - E^2}{X_i} \end{cases} \quad (8)$$

Therefore, the droop characteristics of each micro source can be expressed as:

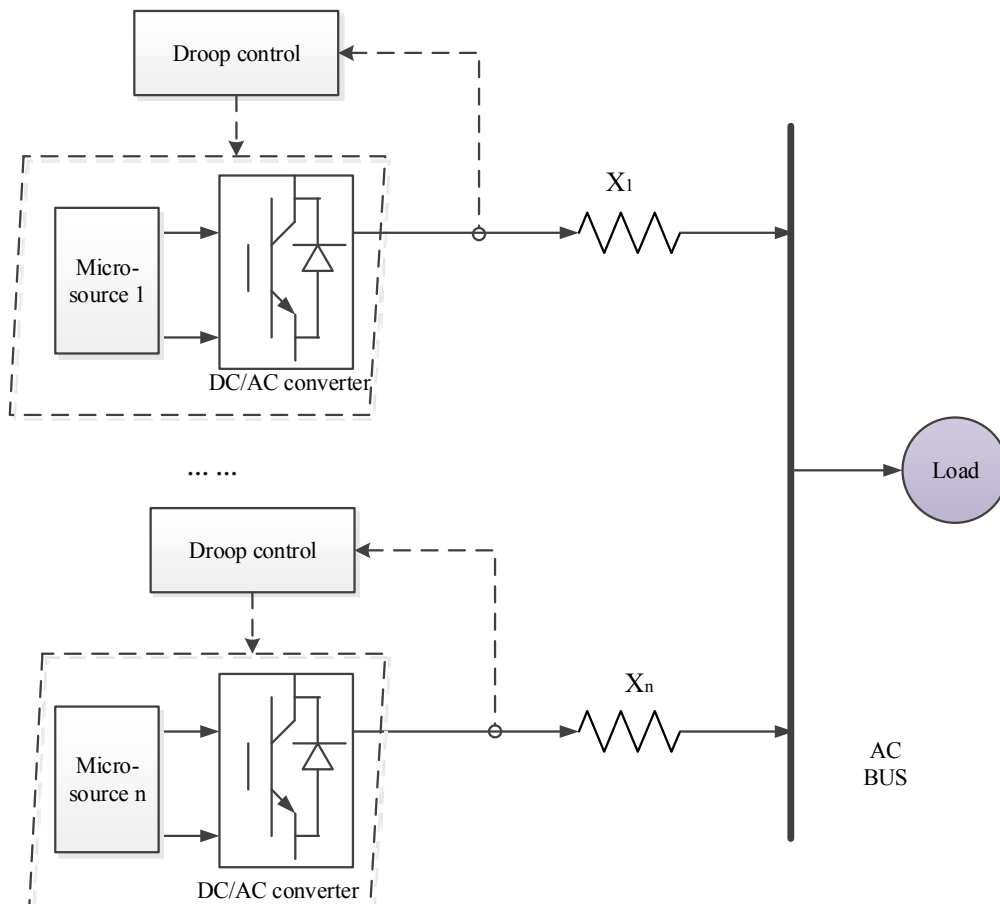


Fig. 2 The simplified structure of AC microgrid in island operation.

$$\begin{cases} f_i = f_n - m_i(P_i - P_{ni}) \\ V_i = V_n - n_i(Q_i - Q_{ni}) \end{cases} \quad (9)$$

$$n_i Q_i = \frac{EV_i - E^2}{\frac{X_i}{n_i}} \quad (11)$$

In the microgrid, the capacity, sag coefficient and line impedance parameters of each micro-source are not consistent, so there are many problems in the integrated control of the system. For the stability of microgrid system, it is expected to output the active and reactive power in proportion to its own capacity in the control of each micro-source. Therefore, each micro source will have almost the same margin to participate in the regulation of microgrid voltage and frequency stability. According to the national standard, the fluctuation range of power grid voltage is 10% and the frequency fluctuation range is 0.5 Hz. The output voltage and frequency range of each micro source in the microgrid are specified by reference to national standards. Therefore, the droop parameters  $m$  and  $n$  corresponding to micro sources with large capacity are relatively small, while droop parameters  $m$  and  $n$  corresponding to micro sources with small capacity are relatively large. In order to ensure that each micro source has the same margin to regulate the grid voltage, the following relationship should be satisfied for each micro source in the microgrid.

$$n_1 Q_1 = n_2 Q_2 = \dots = n_n Q_n \quad (10)$$

Considering the reactive power equation, Eq. (10) can be expressed as:

In Eq. (11),  $EV_i - E^2$  of each micro source are consistent. Therefore, if Eq. (10) is satisfied, it needs:

$$X_1 Q_1 = X_2 Q_2 = \dots = X_n Q_n \quad (12)$$

However, because the distance between each micro source and the AC bus is not consistent, it is difficult to maintain the proportional distribution, so that the output power of each micro source cannot be distributed in a proportional way, and the node voltage of each micro source is not consistent. In the case that the impedance of each micro source does not match, the impedance of the circuit is usually matched by introducing virtual impedance [21]. After virtual impedance is introduced, Eq. (12) can satisfy the proportional distribution, that is:

$$(X_1 + X_{v1})Q_1 = (X_2 + X_{v2})Q_2 = \dots = (X_n + X_{vn})Q_n \quad (13)$$

#### IV. DROOP CONTROL BASED ON VIRTUAL IMPEDANCE

Fig. 3 shows the structure of the micro source converter based on the based on virtual impedance droop control. On the basis of the droop controller, the introduction of virtual impedance control links can adjust the output voltage and frequency reference of the droop controller so that the proportional distribution of reactive power of the micro source can ensure that the AC bus voltage achieves the consistent equilibrium value [22].

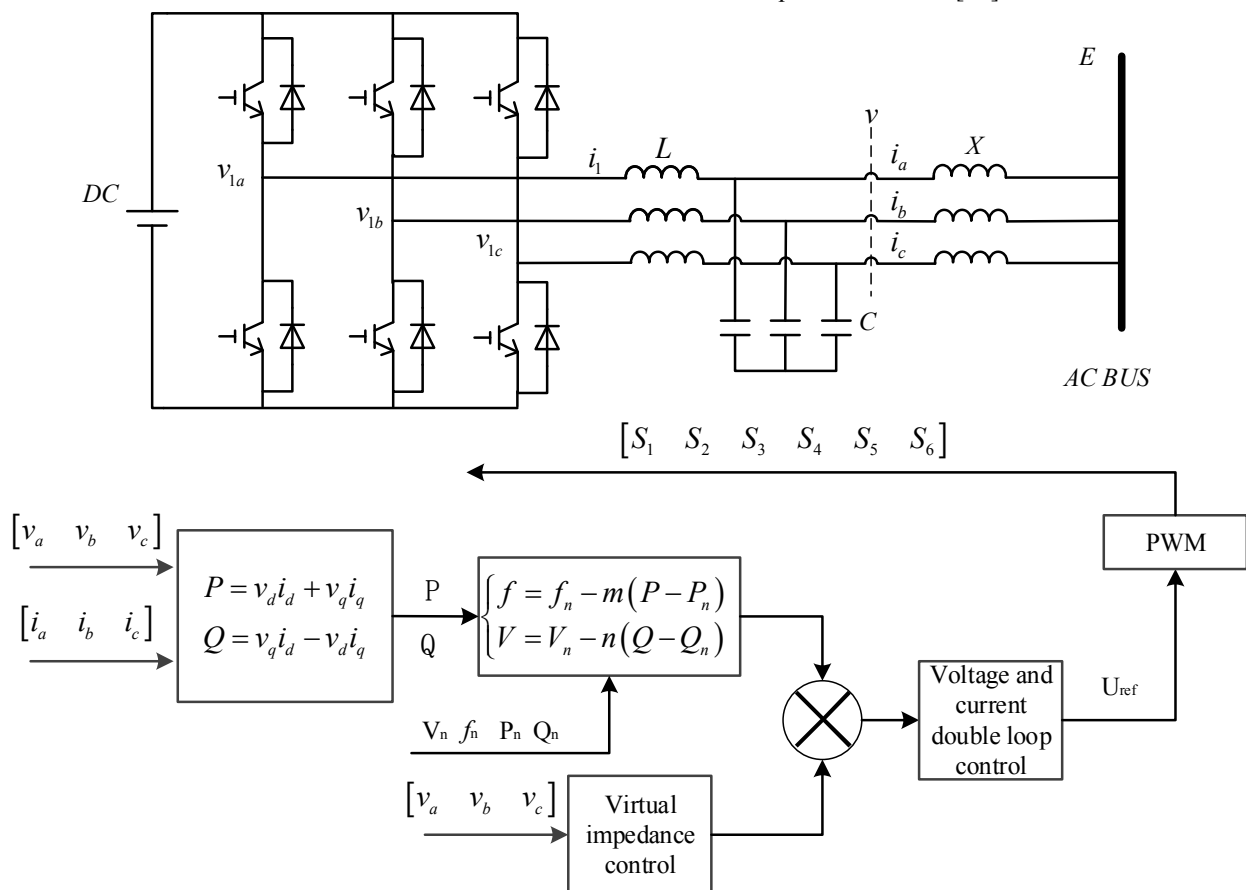


Fig. 3 Block diagram of droop control based on virtual impedance.

Fig. 3 is mainly divided into two parts. The upper part is the micro source converter, which is equivalent to the DC voltage source, the line filtering parameters are  $L$  and  $C$ , and the line inductive reactance parameters are  $X$ . The equivalent output voltage before filtering inductance is  $[v_{1a} \ v_{1b} \ v_{1c}]$ , the equivalent voltage at the filter capacitor is  $[v_a \ v_b \ v_c]$ , the filter inductance current is  $[i_{1a} \ i_{1b} \ i_{1c}]$ , the actual output current of the micro source converter is  $[i_a \ i_b \ i_c]$ , and the voltage at the AC bus is  $[e_a \ e_b \ e_c]$ . The lower part is the control link. According to the droop controller based on virtual impedance, there are three control links: droop controller, virtual impedance controller, and voltage and current double-loop controller. The droop controller provides the basic voltage and frequency reference values, which are modified by the virtual impedance controller, and then the reference voltage is generated by the voltage-current double-loop controller. After PWM processing, the control signal of the micro-source converter is obtained as  $[S_1 \ S_2 \ S_3 \ S_4 \ S_5 \ S_6]$ .

In order to derive the virtual impedance controller, the voltage and current double loop controller and droop controller are designed, and then the virtual impedance controller is introduced. The voltage and current double-loop controller is generally based on the voltage and current feedback at the LC filter, with the inductance current feedback as the current inner loop and the capacitor voltage feedback as the voltage outer loop [23]. Before designing the controller, the mathematical model of the converter should be established. The general mathematical model of micro source converter is the filter mathematical model in the low-frequency mode, namely:

$$L \frac{d}{dt} \begin{bmatrix} i_{1a} \\ i_{1b} \\ i_{1c} \end{bmatrix} = \begin{bmatrix} v_{1a} \\ v_{1b} \\ v_{1c} \end{bmatrix} - \begin{bmatrix} v_a \\ v_b \\ v_c \end{bmatrix} \quad (14)$$

$$C \frac{d}{dt} \begin{bmatrix} u_{1a} \\ u_{1b} \\ u_{1c} \end{bmatrix} = \begin{bmatrix} i_{1a} \\ i_{1b} \\ i_{1c} \end{bmatrix} - \begin{bmatrix} i_a \\ i_b \\ i_c \end{bmatrix} \quad (15)$$

After the rotation transformation on Eq. (14) and Eq. (15), the new mathematical model of micro source converter can be expressed as:

$$L \frac{d}{dt} \begin{bmatrix} i_{1d} \\ i_{1q} \end{bmatrix} = \begin{bmatrix} v_{1d} \\ v_{1q} \end{bmatrix} - \begin{bmatrix} v_d \\ v_q \end{bmatrix} + \begin{bmatrix} 0 & \omega L \\ -\omega L & 0 \end{bmatrix} \begin{bmatrix} i_{1d} \\ i_{1q} \end{bmatrix} \quad (16)$$

$$C \frac{d}{dt} \begin{bmatrix} u_d \\ u_q \end{bmatrix} = \begin{bmatrix} i_{1d} \\ i_{1q} \end{bmatrix} - \begin{bmatrix} i_d \\ i_q \end{bmatrix} + \begin{bmatrix} 0 & \omega C \\ -\omega C & 0 \end{bmatrix} \begin{bmatrix} u_d \\ u_q \end{bmatrix} \quad (17)$$

Therefore, the mathematical model structure of the micro source converter in the rotating coordinate system is shown in Fig. 4.

#### A. Current Loop Controller

The current loop control of the voltage double-loop controller is based on the inductive current feedback.

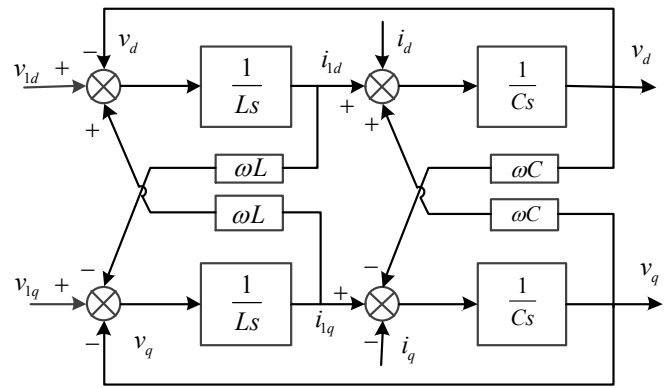


Fig. 4 The math model of micro-source converter.

The mathematical model of the inductive current can be expressed as:

$$\begin{cases} L \frac{di_{1d}}{dt} = v_{1d} - v_d + \omega L i_{1q} \\ L \frac{di_{1q}}{dt} = v_{1q} - v_q - \omega L i_{1d} \end{cases} \quad (18)$$

According to the mathematical model, it can be seen that the micro-source converter has a coupling relationship between  $d$  axis and  $q$  axis in the rotating coordinate system, so how to eliminate the coupling term should be considered in the design of the current loop [24]. Therefore, the current loop control equation is constructed in the controller as follows:

$$\begin{cases} v_{1d} = k(i_{1dref} - i_{1d}) + v_d - \omega L i_{1q} \\ v_{1q} = k(i_{1qref} - i_{1q}) + v_q + \omega L i_{1d} \end{cases} \quad (19)$$

Generally, as the dynamic response speed of the current loop is relatively high, and the integral link in the PI regulator has an impact on the dynamic response, a single  $P$  regulator is generally considered [25]. The control block diagram of the current decoupling controller can be shown in Fig. 5.

The current control block diagram after decoupling can be obtained through Fig. 5, which is shown in Fig. 6, where the current coupling term and voltage coupling term have been eliminated.  $\tau$  is the sampling signal cycle time. At the same time, the simplified decoupling block diagram of current loop needs to consider the delay effect generated by PWM signal, and 0.5 times the sampling cycle time is generally taken.

The open-loop transfer function of the current loop is expressed as:

$$\phi_{oi} = \frac{k}{1 + \tau s} \frac{k_{pwm}}{1 + 0.5\tau s} \frac{1}{Ls} \approx \frac{kk_{pwm}}{(1 + 1.5\tau s)Ls} \quad (20)$$

The sampling frequency of micro source converters is generally 15kHz, so the sampling period is 66.7 $\mu$ s. Assuming that the DC voltage is 700V, the general calculation of the PWM modulator  $k_{pwm}$  is realized by:

$$k_{pwm} = 700 \times 0.866 / \sqrt{3} = 350 \quad (21)$$



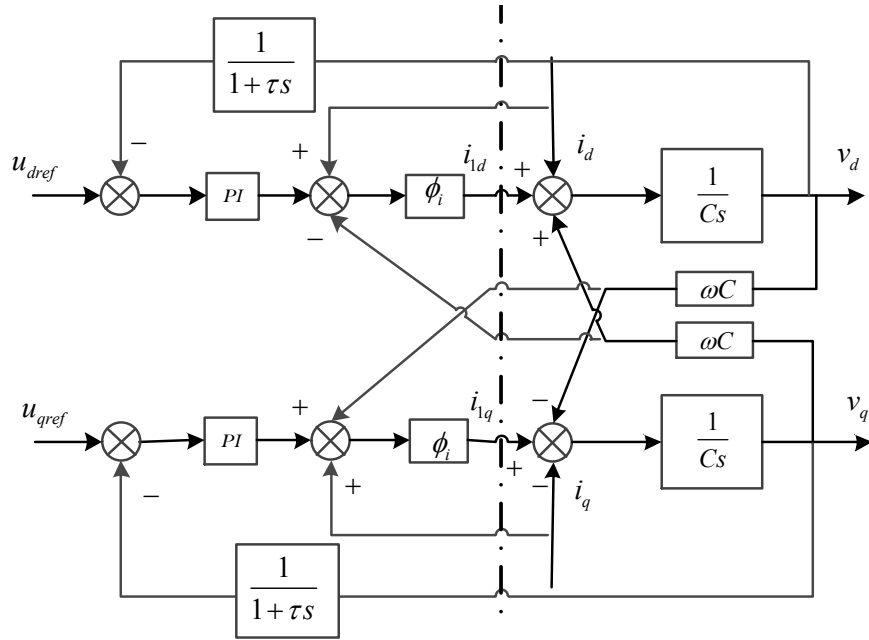


Fig. 7 The control block of voltage loop.

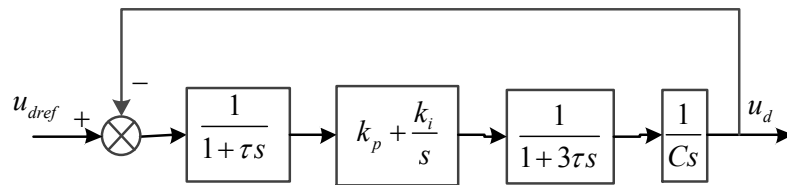


Fig. 8 Simplified block diagram of voltage control.

Generally, the intermediate frequency bandwidth value is 5 and the capacitance value is 10uF. After putting into the above equation, the PI parameters can be obtained by:

$$\begin{cases} k_p = 3C / 20\tau = 0.225 \\ k_i = 3C / 25\tau^2 = 18740 \end{cases} \quad (28)$$

Therefore, the closed-loop transfer function of the voltage loop can be expressed as:

$$\phi_v = \frac{k_p s + k_i}{(1 + 4\tau s)Cs^2 + k_p s + k_i} \quad (29)$$

### C. Droop Controller Based on Virtual Impedance

Due to the inconsistency of line impedance, the reactive power of each micro source does not match, which affects the voltage control at the AC bus. Therefore, the virtual impedance link needs to be introduced to match the impedance of each micro source through the virtual impedance controller [27]. The virtual impedance controller modifies the voltage reference value generated by the droop controller by introducing the voltage drop of virtual impedance and load current, namely:

$$v_{ref} = v_{ref\_droop} + v_v = v_{ref\_droop} + i\omega L_v \quad (30)$$

It is converted under dq coordinate system as:

$$\begin{cases} v_{dref} = v_{dref\_droop} + v_{dv} = v_{dref\_droop} - \omega L_v i_d \\ v_{qref} = v_{qref\_droop} + v_{qv} = v_{dref\_droop} + \omega L_v i_q \end{cases} \quad (31)$$

After the virtual impedance controller is introduced, the structure of the voltage and current double-loop controller is shown in Fig. 9. After the virtual impedance correction, the voltage reference value is obtained as  $v_{dref}$  and  $v_{qref}$ . Then a new PWM reference value  $U_{ref}$  is generated by voltage-current double-loop controller, which can adjust the system output reactive power matching.

In order to compare and analyze the effect of virtual impedance on the output characteristics of inverter, the bode diagram of current loop and voltage loop without virtual impedance is firstly analyzed. According to the current open-loop transmission function shown in Eq. (20), the data are fed to obtain the open-loop bode diagram shown in Fig. 10. The corresponding phase margin at the cut-off frequency is 57 degree, so the system is stable. At the same time, the system crosses the medium frequency band with 20dB/dec, which has good dynamic performance. According to the voltage open-loop transmission function described in Eq. (26), the data are fed to obtain the open-loop bode diagram shown in Fig. 11. The corresponding phase margin at the cut-off frequency is 40 degree, so the system is stable. At the same time, the system crosses the medium frequency band with 30dB/dec and has good dynamic performance.

Before virtual impedance is introduced, the output voltage equation of the controller can be expressed as:

$$u_d = u_{dref} \phi_v - i_d Z_i \quad (32)$$

where,  $Z_i$  is the output impedance of micro source converter.

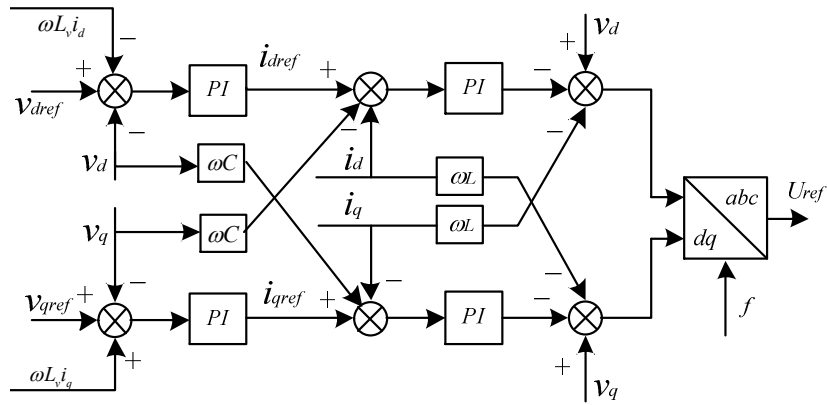


Fig. 9 The voltage and current control based on virtual impedance.

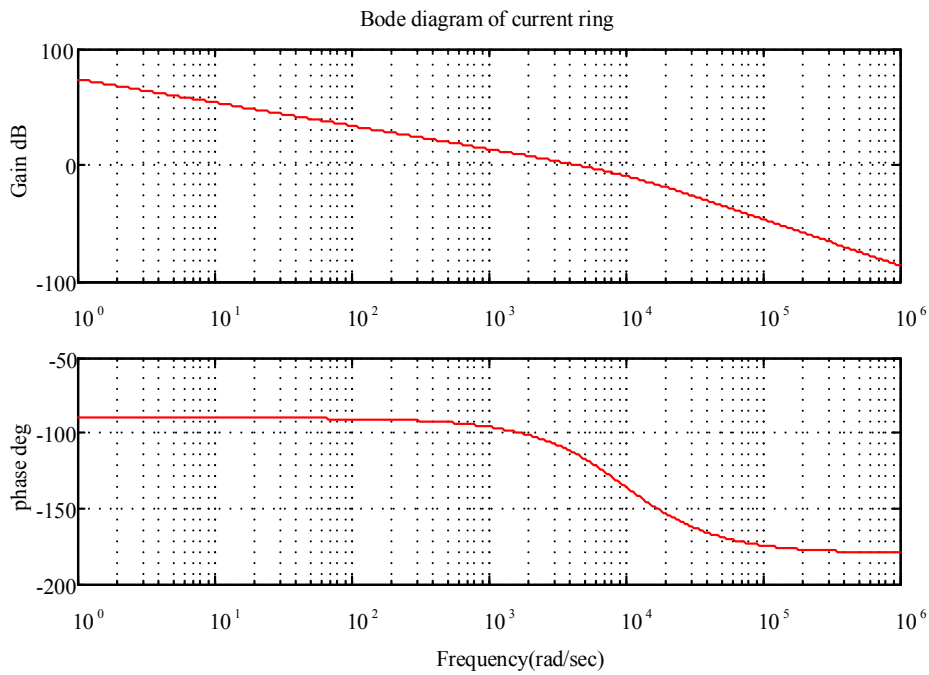


Fig. 10 The bode diagram of current loop.

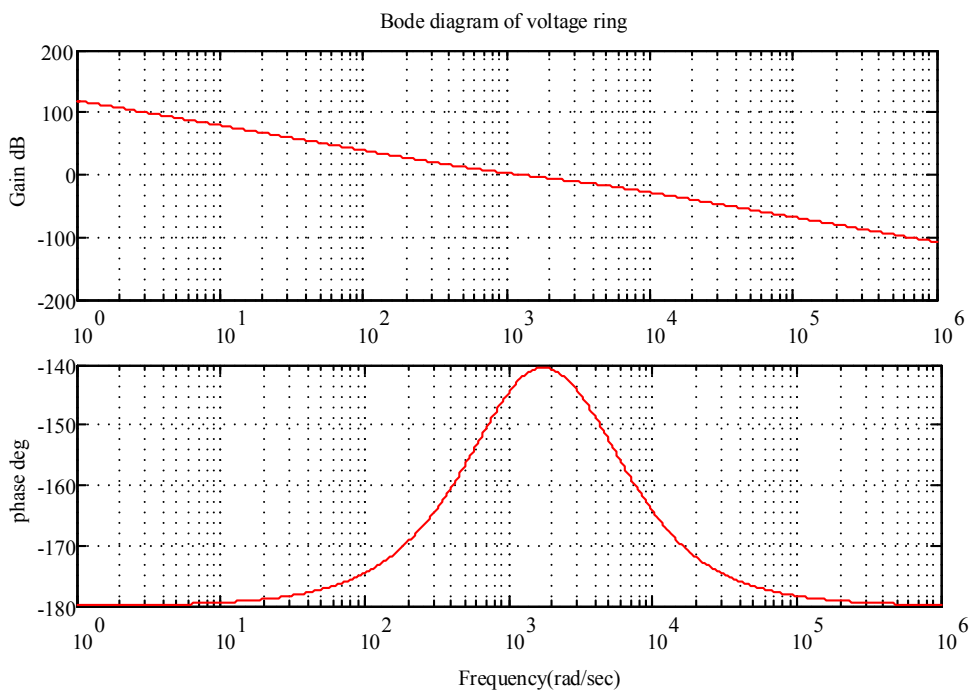


Fig. 11 The bode diagram of voltage loop.

So the impedance equation can be expressed as:

$$Z_i = \frac{(1+4\tau s)s}{(1+4\tau s)Cs^2 + k_p s + k_i} \quad (33)$$

According to the bode diagram of the output impedance  $Z_i$  shown in Fig. 12, it can be seen that the output impedance shows impedance characteristics under the power network frequency rate, so the regulation of system voltage requires both active power and reactive power. Therefore, under the premise of ensuring voltage stability, it is impossible to realize the average distribution of reactive power. The transfer block diagram of voltage and current loop with virtual impedance is shown in Fig. 13.

According to Eq. (20), Eq. (26) and Fig. 11, the output voltage equation of the controller based on virtual impedance can be deduced as follows:

$$\begin{aligned} u_d &= (u_{dref\_droop} - \omega L_v i_d) \phi_v - i_d Z_i \\ &= u_{dref\_droop} \phi_v - i_d (\omega L_v \phi_v + Z_i) \end{aligned} \quad (34)$$

Since the virtual impedance term is equivalent to the disturbance term for the control loop, it does not affect the

transfer functions of the voltage loop and current loop, but the output impedance equation of the system changes. The virtual impedance equation can be expressed as:

$$Z_{vi} = \omega L_v \phi_v + Z_i = \frac{(k_p s + k_i) \omega L_v + (1+4\tau s)s}{(1+4\tau s)Cs^2 + k_p s + k_i} \quad (35)$$

Suppose that the introduced virtual impedance is 3.3mH, then the amplitude-frequency characteristics of the virtual impedance is shown in Fig. 14. According to the bode diagram of output impedance  $Z_i$ , it can be seen that the output impedance exhibits inductive reactance characteristics under the power network frequency, so the regulation of system voltage is only related to reactive power [28]. Therefore, the reactive power can be equally divided by virtual impedance, and the output characteristics of reactive power and voltage can be guaranteed at the same time.

Therefore, after the introduction of the virtual impedance, the equivalent circuit of the micro-source is shown in Fig. 15, where the line keep pure emotion. Introducing the virtual impedance at the same time satisfies the proportional distribution of reactive power shown in Eq. (13), which ensures that each micro-source system has the voltage stability margin for AC bus-bar and enhances the stability of the microgrid operation [29].

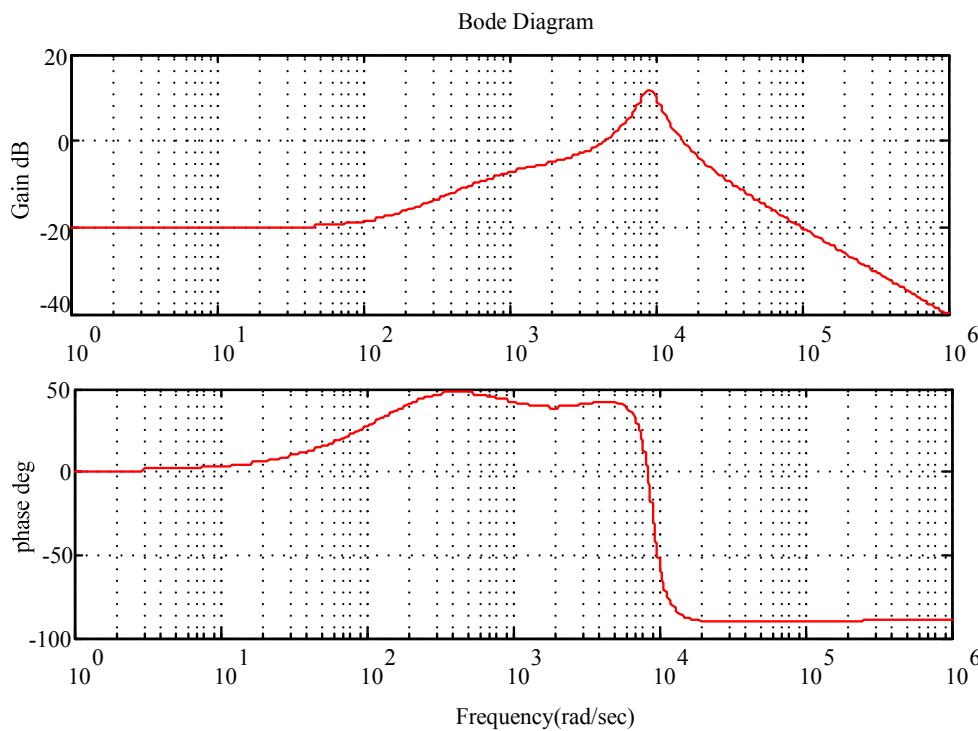


Fig. 12 The bode diagram of output impedance  $Z_i$ .

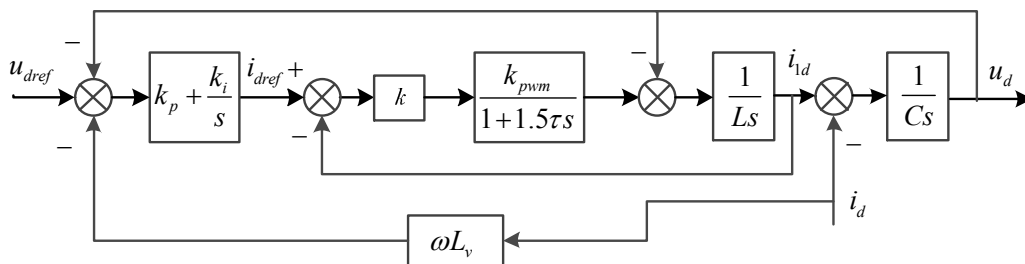


Fig. 13 Block diagram of voltage current loop transfer with virtual impedance.

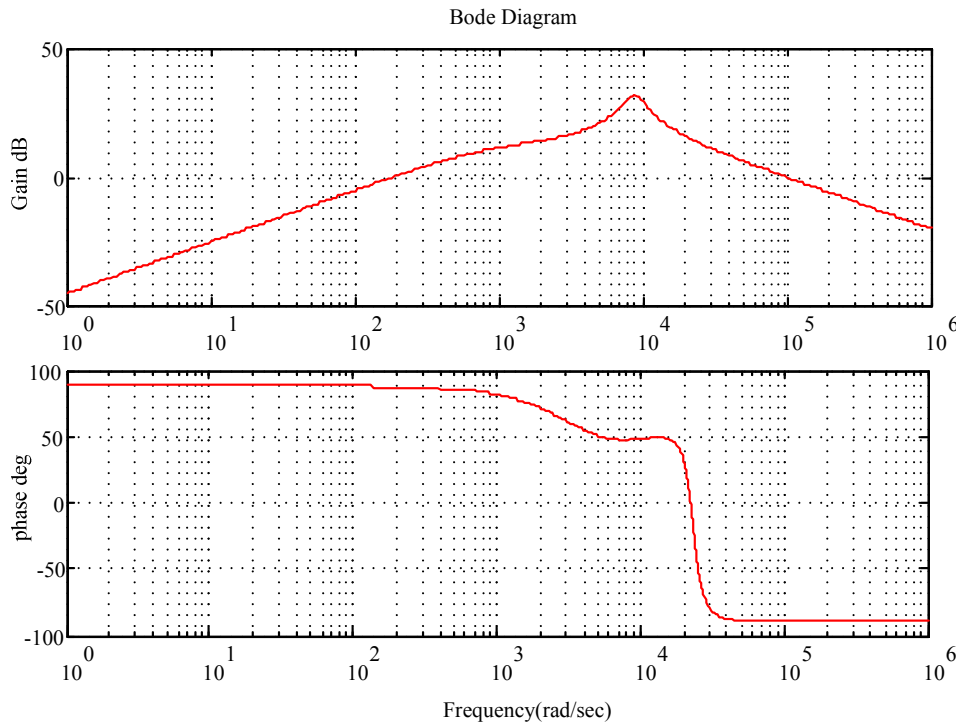


Fig. 14 The bode diagram of output impedance  $Z_i$  with virtual impedance.

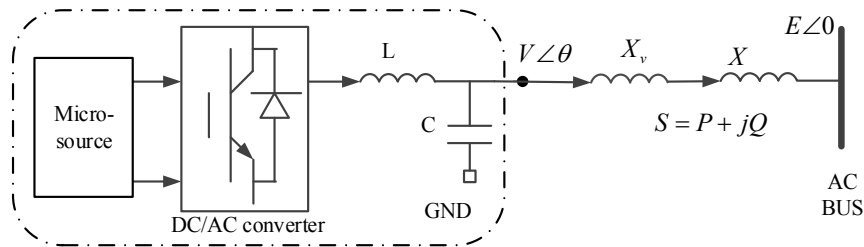


Fig. 15 The equivalent circuit of micro source with virtual impedance.

V. SIMULATION EXPERIMENTS AND RESULTS ANALYSIS

Parameters and conditions of MATLAB simulation model using virtual impedance are shown in Table 1. There are three micro-source converters in the microgrid, which are called DG1, DG2 and DG3 respectively, and their capacity ratio is 1:2:3. At the same time, three groups of loads were set, and their capacities were respectively  $S1=9kW + j4.5kvar$ ,  $S2=6.75kw + j2.25kvar$ , and  $S3=6.75kw + j4.5kvar$ . Load S1 is connected to the microgrid at the initial moment, load S2 is connected to the microgrid at 0.2s, and load S3 is connected to the microgrid at 0.4s. Fig. 16 shows the load power curve at the micro source AC bus. It can be seen that load power changes when load S2 and S3 are connected at 0.2s and 0.4s. Fig. 17 is a peer-to-peer control mode, and the traditional droop control strategy is adopted to obtain the reactive power waveform by each distributed micro-source. According to the waveform, the reactive power by each micro-source converter is not effectively distributed according to its capacity when the load is increased.

In order to realize the proportional distribution of reactive power, a virtual impedance controller is introduced. By adjusting the line impedance parameters, the reactive capacity and line impedance parameters of each micro source are kept at a fixed value, so as to realize the proportional distribution of reactive power.

TABLE 1. SIMULATION MODEL PARAMETERS

Parameter	Value	Parameter	Value
PI parameters of voltage loop	$K_p=0.2$ $K_i=200$	PI parameters of current loop	$K_p=0.0471$
AC reference voltage	400V	Reference frequency	50Hz
DG1 frequency drop coefficient	$6e-5$	DG1 voltage sag factor	$3e-4$
DG2 frequency drop coefficient	$4e-5$	DG2 voltage sag factor	$2e-4$
DG3 frequency drop coefficient	$3e-5$	DG3 voltage sag factor	$1.5e-4$
DG1 capacity	$P=6kW$ $Q=3kVar$	DG1 impedance	9mH
DG2 capacity	$P=9kW$ $Q=4.5kVar$	DG2 impedance	7.3mH
DG3 capacity	$P=12kW$ $Q=6kVar$	DG3 impedance	5.8mH
DG1 virtual impedance	3mH	DG2 virtual impedance	0.7mH
DG3 virtual impedance	0.2mH	DC bus voltage	700V

As shown in Fig. 18, after adopting the virtual impedance controller, when the load changes, the reactive power output of micro source DG1, DG2 and DG3 is distributed according to its own capacity, and the distribution ratio is 1:1.5:2. At load S1, the output power of DG1 is 1kvar, the output power of DG2 is 1.5kvar, and the output power of DG3 is 2kVar. When loading S2, the output power of DG1 is 1.5kvar, the output power of DG2 is 2.5kvar, and the output power of DG3 is 3.5kvar. For load S3, the output power of DG1 is 2.5kvar, the output power of DG2 is 4kVar, and the output power of DG3 is 5.5kvar. By comparing the simulation results, it can be seen that the droop control strategy based on

virtual impedance can realize the proportional analysis of reactive power.

The established MATLAB models are mainly to verify in the microgrid with multi-converter parallel connection, the inconsistent line impedance will make the peer-to-peer control based on traditional droop method not realize the proportional equalization of reactive power output of each converter in the microgrid. The droop control method based on the virtual impedance can adjust the output impedance characteristics to realize the matching of reactive power output for each converter and the stability of voltage regulation in microgrid.

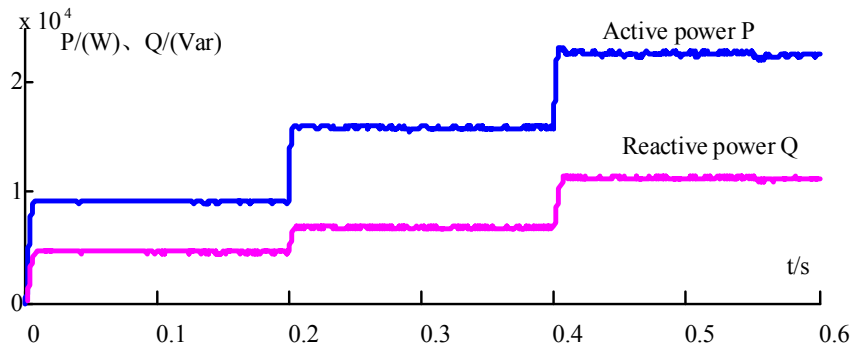


Fig. 16 The power curves of AC load.

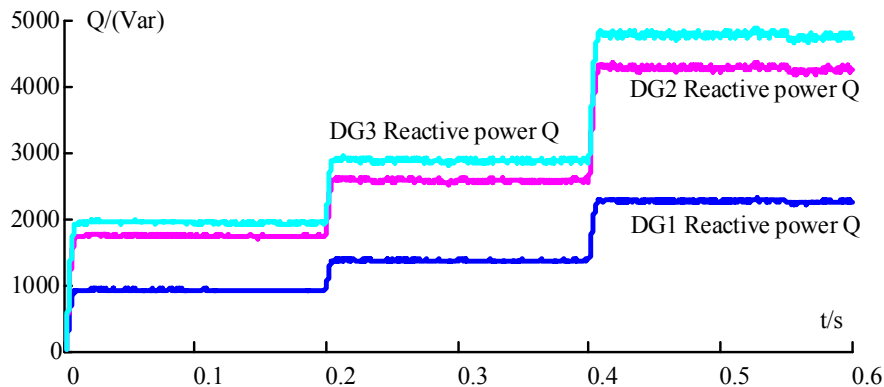


Fig. 17 The reactive power waves in traditional droop control.

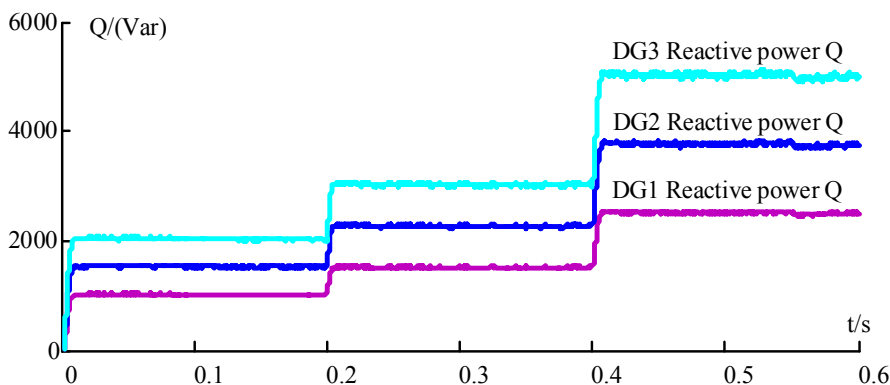


Fig. 18 The reactive power waves in droop control with virtual impedance.

VI. CONCLUSION

This paper mainly studies the voltage relationship between the reactive power of microgrid and the AC bus in off-grid operation mode. Due to the inconsistency of line impedance, the reactive power cannot be distributed according to its

capacity when the traditional droop control strategy is adopted in the voltage regulation. Therefore, a microgrid droop control strategy based on virtual impedance is adopted. By introducing a virtual impedance controller and combining the control layer and the electrical layer, the line impedance satisfies the condition of proportional distribution of reactive power, so as to realize the optimal regulation of microgrid

voltage. Finally, MATLAB simulation results are used to verify the reactive power distribution strategy of microgrid based on the virtual impedance proposed in this paper.

## REFERENCES

- [1] J. W. Cao, K. Meng, J. Y. Wang, M. B. Yang, Z. Chen, W. Z. Li, and C. Lin, "An Energy Internet and Energy Routers," *Scientia Sinica (Informationis)*, vol. 44, no. 6, pp. 714-727, 2014.
- [2] S. Tian, W. Luan, D. Zhang, C. Liang, and Y. Sun, "Technical Forms and Key Technologies on Energy Internet," *Proceedings of the Chinese Society of Electrical Engineering*, vol. 35, no. 14, pp. 3482-3494, 2015.
- [3] J. L. Li, L. T. Tian, and X. K. Lai, "Outlook of Electrical Energy Storage Technologies Under Ender Internet Background," *Automation of Electric Power Systems*, vol. 23, pp. 15-25, 2015.
- [4] F. Nejabatkhah, and Y. W. Li, "Overview of Power Management Strategies of Hybrid AC/DC Microgrid," *IEEE Transactions on Power Electronics*, vol. 30, no. 12, pp. 7072-7089, 2015.
- [5] W. H. Cui, J. S. Wang, and Y. Y. Chen, "Equivalent Circuit Model of Lead-acid Battery in Energy Storage Power Station and its State-of-Charge Estimation Based on Extended Kalman Filtering Method," *Engineering Letters*, vol. 26, no. 4, pp. 504-517, 2018.
- [6] H. Morais, Kádár Péter, P. Faria, Z. A. Vale, and H. M. Khodr, "Optimal Scheduling of a Renewable Microgrid in an Isolated Load Area Using Mixed-integer Linear Programming," *Renewable Energy*, vol. 35, no. 1, pp. 151-156, 2010.
- [7] X. Z. Yang, S. U. Jian-Hui, M. Ding, and D. U. Yan, "Research on Frequency Control for Microgrid in Islanded Operation," *Power System Technology*, vol. 34, no. 1, pp. 164-168, 2010.
- [8] M. Ding, L. G. Tian, H. Pan, X. S. Zhang, and J. H. Zhou, "Research on Control Strategy of Hybrid AC/DC Microgrid," *Power System Protection and System*, vol. 43, no. 9, pp. 1-8, 2015.
- [9] Y. C. Xue, N. L. Tai, L. Q. Liu, X. W. Yang, N. Jin, and N. Xiong, "Co-operation Control Strategies for Islanded Microgrids," *Electric Power*, vol. 42, no. 7, pp. 36-40, 2009.
- [10] W. Liu, "A Study of Master-slave Control Strategy in Isolated Microgrid," *Journal of WuYi University*, vol. 25, no. 3, pp. 56-60, 2011.
- [11] Y. S. Chen, P. Yang, Z. J. Zeng, and J. J. Peng, "Planning of Distributed Energy Resources for Distribution Network Considering Dispatchable Region of Microgrids," *Automation of Electric Power Systems*, vol. 43, no. 3, pp. 83-91, 2019.
- [12] J. J. Jiang, and R. Ju, "Summary of Microgrid Control Technology," *Advanced Materials Research*, vol. 1070-1072, pp. 1326-1334, 2015.
- [13] X. Zhu, J. Liu, Y. Liu, Y. Xiang, and H. Tian, "Study of Microgrid Control Strategy Contained Unbalanced Load Based on Sliding-mode Variable Structure," *Power System Protection and Control*, vol. 43, no. 6, pp. 25-32, 2015.
- [14] P. M. S. Carvalho, P. F. Correia, and L. A. F. M. Ferreira, "Distributed Reactive Power Generation Control for Voltage Rise Mitigation in Distribution Networks," *IEEE Transactions on Power Systems*, vol. 23, no. 2, pp. 766-772, 2008.
- [15] A. I. Xin, J. Peng, and Y. Y. Sun, "An Enhanced Reactive Sharing Control Strategy of Microgrid," *Power System Protection and System*, vol. 41, no. 7, pp. 147-155, 2013.
- [16] F. C. Lu, and Y. Y. Hsu, "Fuzzy Dynamic Programming Approach to Reactive Power/Voltage Control in a Distribution Substation," *IEEE Transactions on Power Systems*, vol. 12, no. 2, pp. 681-688, 1997.
- [17] F. C. Lu, and Y. Y. Hsu, "Reactive Power/Voltage Control in a Distribution Substation Using Dynamic Programming," *Generation, Transmission and Distribution, IET Proceedings*, vol. 142, no. 6, pp. 639-645, 1995.
- [18] B. Lu, and N. Yi, "A Self-approximate-optimal Distributed Reactive Power and Voltage Control Strategy for Microgrid in Island Mode," *Automation of Electric Power Systems*, vol. 38, no. 9, pp. 218-225, 2014.
- [19] L. Chen, J. Zhong, Y. Ni, D. Gan, J. Xiong, and X. Xia, "Optimal Reactive Power Planning of Radial Distribution Systems with Distributed Generation," *Automation of Electric Power Systems*, vol. 30, no. 14, pp. 20-24, 2006.
- [20] Y. Deng, X. Ren, C. Zhao, and D. Zhao, "A Heuristic and Algorithmic Combined Approach for Reactive Power Optimization with Time-varying Load Demand in Distribution Systems," *Power Systems IEEE Transactions on*, vol. 17, no. 4, pp. 1068-1072, 2002.
- [21] P. R. Laframboise, G. Ferland, A. Y. Chikhani, and M. M. A. Salama, "An Expert System for Reactive Power Control of a Distribution System. Part 2: System Implementation," *IEEE Transactions on Power Systems*, vol. 10, no. 3, pp. 1433-1441, 1995.
- [22] Y. X. Zhu, F. Zhuo, F. Wang, and B. Q. Liu, "Virtual Impedance Optimization Method for Microgrid Reactive Power Balance Control," *Chinese Journal of Electrical Engineering*, vol. 36, no. 17, pp. 4552-4563, 2016.
- [23] S. N. Singh, and S. C. Srivastava, "Improved Voltage and Reactive Power Distribution Factors for Outage Studies," *IEEE Transactions on Power Systems*, vol. 12, no. 3, pp. 1083-1093, 1997.
- [24] J. He, and Y. W. Li, "Analysis, Design, and Implementation of Virtual Impedance for Power Electronics Interfaced Distributed Generation," *IEEE Transactions on Industry Applications*, vol. 47, no. 6, pp. 2525-2538, 2012.
- [25] J. He, and Y. W. Li, "Generalized Closed-Loop Control Schemes with Embedded Virtual Impedances for Voltage Source Converters with LC or LCL Filters," *IEEE Transactions on Power Electronics*, vol. 27, no. 4, pp. 1850-1861, 2012.
- [26] J. He, Y. W. Li, J. M. Guerrero, F. Blaabjerg, and J. C. Vasquez, "An Islanding Microgrid Power Sharing Approach Using Enhanced Virtual Impedance Control Scheme," *IEEE Transactions on Power Electronics*, vol. 28, no. 11, pp. 5272-5282, 2013.
- [27] R. Q. Wang, Y. Cheng, S. M. Sun, Z. X. Jin, B. X. Li, and C. Y. LI, "Microgrid Control and Performance Analysis Based on Coordinate Rotation Virtual Impedance," *Power System Protection and Control*, vol. 42, no. 12, pp. 78-86, 2014.
- [28] W. H. Cui, J. S. Wang, and Y. Y. Chen, "Design and Performance Testing of Lead-acid Battery Experimental Platform in Energy Storage Power Station," *IAENG International Journal of Computer Science*, vol. 44, no. 4, pp. 471-481, 2017.
- [29] W. Bao, X. H. Hu, G. H. Li, and W. Y. Bao, "Improved Drooping Control Based on Virtual Impedance in Independent Micro-grid," *Power System Protection and Control*, vol. 41, no. 16, pp. 7-13, 2013.
- [30] Q. P. Mai, and M. Chen, "Virtual Impedance Anti-droop Control for Multi-micro-source Low-voltage Micro-grid," *Power System Protection and Control*, vol. 46, no. 1, pp. 96-102, 2018.

**Xue-Long Li** is a postgraduate student in the School of Electronic and Information Engineering, University of Science and Technology Liaoning, Anshan, 114051, PR China. His main research interest is modeling of complex industry process, intelligent control and Computer integrated manufacturing.

**Shuang Zhao** is an engineer of Anshan Power Supply Company, State Grid Liaoning Electric Power Co. LTD., Anshan, 114051, PR China. Her main research interest is modeling and control methods of microgrid.

**Jie-Sheng Wang** received his B. Sc. And M. Sc. degrees in control science from University of Science and Technology Liaoning, China in 1999 and 2002, respectively, and his Ph. D. degree in control science from Dalian University of Technology, China in 2006. He is currently a professor and Master's Supervisor in School of Electronic and Information Engineering, University of Science and Technology Liaoning. His main research interest is modeling of complex industry process, intelligent control and Computer integrated manufacturing.

**An He** is an engineer of Anshan Power Supply Company, State Grid Liaoning Electric Power Co. LTD., Anshan, 114051, PR China. His main research interest is modeling and control methods of microgrid.